

Parity violation effects in helical osmocene: theoretical analysis and experimental prospects

Eduardus,¹ Agathe Bonifacio,² Mathieu Manceau,² Naoya Kuroda,³ Masato Senami,³ Juan J. Aucar,⁴ I. Agustín Aucar,^{1,4} Marit R. Fiechter,⁵ Trond Saue,⁶ Jeanne Crassous,⁷ Benoît Darquié,² Shirin Faraji,^{8,9} Lukáš F. Pašteka,^{1,10} and Anastasia Borschevsky^{1, a)}

¹⁾ *Van Swinderen Institute for Particle Physics and Gravity (VSI), University of Groningen, Groningen, The Netherlands.*

²⁾ *Laboratoire de Physique des Lasers, CNRS, Université Sorbonne Paris Nord, Villetaneuse, France.*

³⁾ *Department of Micro Engineering, Kyoto University, Kyoto 615-8540, Japan.*

⁴⁾ *Instituto de Modelado e Innovación Tecnológica (UNNE-CONICET), Facultad de Ciencias Exactas y Naturales y Agrimensura, Universidad Nacional del Nordeste, Av. Libertad 5460, Corrientes, Argentina.*

⁵⁾ *Department of Chemistry and Applied Biosciences, ETH Zürich, 8093 Zürich, Switzerland.*

⁶⁾ *Laboratoire de Chimie et Physique Quantiques, UMR 5626 CNRS – Université de Toulouse, 31062 Toulouse Cedex 09, France.*

⁷⁾ *Université de Rennes, CNRS, ISCR-UMR 6226, Campus de Beaulieu, 35042 Rennes Cedex, France.*

⁸⁾ *Zernike Institute for Advanced Materials, University of Groningen, Groningen, The Netherlands*

⁹⁾ *Institute of Theoretical and Computational Chemistry, Heinrich Heine University Düsseldorf, Universitätsstraße 1, 40225 Düsseldorf, Germany.*

¹⁰⁾ *Department of Physical and Theoretical Chemistry, Faculty of Natural Sciences, Comenius University, Bratislava, Slovakia.*

(Dated: March 9, 2026)

We present a computational investigation of the parity-violating (PV) contributions to the vibrational transitions and nuclear magnetic resonance shieldings of helical osmocene. A number of promising transitions within the spectral window of currently available sub-Hz metrology-grade lasers are identified, exhibiting high intensities and parity violation shifts of up to 7 Hz. We discuss the prospects for the synthesis of this compound and for subsequent ultra-precise mid-IR spectroscopy towards the first detection of parity violation in a chiral molecule.

I. INTRODUCTION

Chirality has a crucial effect on biological processes in living organisms. One of the greatest unresolved questions in biology is the emergence of bihomochirality: in almost all known biological systems, the most important building blocks, amino acids and sugars, occur naturally only in one enantiomer (D-sugars and L-amino acids), while the other enantiomer is biologically incompatible.^{1–3} One of the hypotheses that aims to resolve the mystery of bihomochirality^{4,5} proposes that this is due to a tiny parity-violating energy difference between the two enantiomers. This energy difference may have resulted in a tiny excess of one enantiomer over the other in an originally racemic (equal-handed) prebiotic soup, which, amplified over time, may have led to dominance of one of the enantiomers over the other.^{6–8} While this hypothesis is heavily debated,^{9,10} the existence of molecular parity violation itself has a firm foundation in particle physics, which predicts that the weak interac-

tions between the electrons and the quarks inside the nuclei should result in a small energy difference between the two enantiomers.^{11,12} Parity violation was successfully demonstrated in nuclear¹³ and atomic experiments.^{14,15} Unfortunately, this is not the case with molecular parity violation, despite many years of attempts using a variety of experimental techniques.^{16–20}

The only experiments so far to have set a strict upper bound on PV effects in chiral molecules were performed at the Laboratoire de Physique des Lasers (LPL) in Paris,^{16,21} using ultra-precise mid-infrared spectroscopy experiments on rovibrational transitions. These measurements were performed on the C–F stretch vibration in the archetypal chiral molecule CHFClBr, setting a limit of $\Delta\nu^{\text{PV}}/\nu = 2.5 \times 10^{-13}$ on the relative PV frequency shift (with ν the vibrational transition frequency and $\Delta\nu^{\text{PV}}$ the upper limit of the PV frequency difference between the enantiomers, corresponding to about 8 Hz in this case). Subsequent computational studies, however, showed that the actual expected relative PV difference for this transition is a few orders of magnitude smaller (10^{-17}) and could not have been reached within the precision of these measurements.^{22–26}

Currently, there is an ongoing attempt to measure PV shifts in vibrational spectra of chiral molecules using an

^{a)} **Author to whom correspondence should be addressed:** a.borschevsky@rug.nl

ultrahigh resolution gas-phase spectroscopy experiment based on metrology-grade lasers in the 500–2000 cm^{-1} range at LPL.^{27–29} The current set-up is expected to reach relative PV frequency shift sensitivity on the order of 10^{-15} ; therefore, a candidate molecule is needed where the expected PV frequency shift is at least in the order of magnitude of hundreds of mHz to Hz. Additionally, there are practical requirements such a molecule should satisfy – it should be possible to bring it into the gas phase while maintaining chemical stability, it should ideally be possible to separate it into pure enantiomers, and it should have strong vibrational transitions in a range accessible to current laser technologies. Furthermore, such a molecule should contain heavy elements, as the absolute PV energy is predicted to scale as $\sim Z^5$.^{30,31} These criteria can guide the initial selection of the molecular candidates. However, to evaluate the size of PV shifts in various vibrational transitions and to select the optimal transitions for measurements, explicit electronic structure calculations are necessary.

In this work, we investigate helicenic organometallic metallocene-type complexes displayed in Figure 1, formed by metal coordination of a ligand having seven *ortho*-fused aromatic rings including terminal cyclopentadienyl rings. These compounds exhibit inherent helical chirality. While the enantiopure forms of the heptahelicenic ligand may undergo partial racemization, especially at high temperatures,^{32,33} complexation by a metal will increase the overall configurational stability.³⁴ Upon binding to Fe(II), helical ferrocene, an η -10 type complex, was readily synthesized by Katz and Pesti in 1982,³⁵ characterized by X-ray crystallography in 1983,³⁶ prepared in enantioenriched form, and its chiroptical properties studied in 1986.³⁷ In principle, the preparation of heavier homologues, namely ruthenium and osmium complexes as depicted in Figure 1, may be considered. The size of the PV energy differences is expected to be amplified in these heavier compounds.^{30,31,38}

We present a computational investigation of the parity-violating contributions to the vibrational transitions and nuclear magnetic resonance (NMR) shieldings of helical ferrocene, ruthenocene, and osmocene. We aim to determine whether the expected effects are large enough to be detectable in a modern, state-of-the-art experiment. We identify the vibrational transitions that are most promising for measurements, due to enhanced PV effects and practical considerations, such as high enough transition intensities and wavelengths that are easily accessible to current laser technologies. Progress in the development of the ultra-precise experiment dedicated to PV measurements is also presented.

II. THEORY AND COMPUTATIONAL DETAILS

The geometry optimization and the harmonic frequency analysis were carried out using the Q-Chem 5.2.2 program,³⁹ within the ω B97M-V density functional⁴⁰

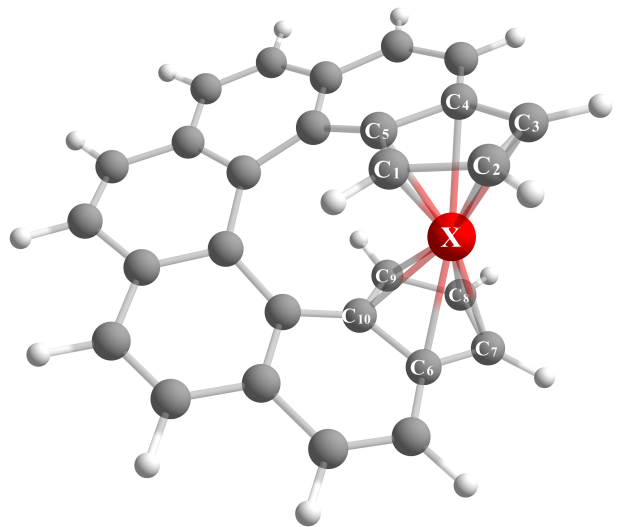


Figure 1. Helical metallocene structure (X = Fe/Ru/Os) with 10 connected carbon atoms (η -10 complex).

combined with the Def2-TZVPP basis set,⁴¹ which includes triple- ζ valence (TZV) functions and large polarization functions (PP), together with the Stuttgart–Dresden small-core scalar-relativistic ECP n MWB pseudopotentials replacing the inner $n = 28, 60$ electrons for Ru and Os, respectively.⁴²

A. PV in vibrational transitions

We investigated the PV effects for vibrational modes 9–129 for helical osmocene (Table S1 in ESI[†]), and compared selected modes 102, 103, and 108 with helical ruthenocene and ferrocene. For each mode, energy calculations were performed along the normal mode at 11 evenly spaced points q_i between -0.5 \AA and 0.5 \AA (relative to the equilibrium structure) to obtain the potential energy curve $V(q)$, using the same level of theory as the geometry optimization.

We have also calculated the PV energy contributions at the same geometries along the normal mode, using the nuclear spin-independent (NSI) PV Hamiltonian as derived from the Z boson exchange between the electrons and nucleons:^{31,43}

$$\hat{H}^{\text{NSI-PV}} = \frac{G_{\text{F}}}{2\sqrt{2}} \sum_A Q_{\text{w},A} \sum_i \gamma_i^5 \rho_A(\vec{r}_i). \quad (1)$$

Here, $G_{\text{F}} = 2.22255 \times 10^{-14}$ a.u. is the Fermi coupling constant, $Q_{\text{w},A} = (1 - 4 \sin^2 \theta_{\text{W}}) Z_A - N_A$ is the weak charge of nucleus A , θ_{W} is the Weinberg mixing angle (with $\sin^2 \theta_{\text{W}} = 0.2319$ value adopted in DIRAC19),^{44,45} and Z_A and N_A are the proton and neutron numbers of nucleus A , respectively. The sums over indices A and i run over all nuclei and electrons, respectively. We

also define $\gamma^5 = i\gamma^0\gamma^1\gamma^2\gamma^3$, and $\rho_A(\vec{r})$ denotes the nuclear charge density of nucleus A normalized such that $\int \rho_A(\vec{r})d^3r = 1$.

Treating $\hat{H}^{\text{NSI-PV}}$ as a first-order perturbation, the PV energy shift—at a given point along the normal coordinate q —is given by the expectation value $E^{\text{PV}} = \langle \Psi^{\text{el}} | H^{\text{NSI-PV}} | \Psi^{\text{el}} \rangle$, which holds for stationary Hartree–Fock (HF) or density functional theory (DFT) solutions.^{46,47} The E^{PV} values are obtained using the X2C/AMFI Hamiltonian^{48,49}. In particular, the CAM-B3LYP* DFT functional⁵⁰, which is optimized for PV calculations, combined with the augmented uncontracted dyall.v3z⁵¹ basis set for the heavy metals and dyall.v2z⁵² for the other atoms were used. These calculations were performed using the DIRAC19 program^{45,53}.

To obtain the PV shift for a specific vibrational mode, we used the numerical Numerov–Cooley (NC) procedure.^{54–56} Both the potential energy $V(q)$ and the PV energy contribution $E^{\text{M,PV}}(q)$ for the minus enantiomer (M) were fitted to a polynomial up to the sixth order. For a given normal mode, the vibrational wavefunction of the n -th vibrational energy level, $|n\rangle$, was obtained numerically and this was subsequently used for the calculation of PV energy contribution to the vibrational energy level ($E_n^{\text{M,PV}}$):

$$E_n^{\text{M,PV}} = \langle n | E^{\text{M,PV}}(q) | n \rangle. \quad (2)$$

The PV energy shift for a vibrational transition $n \rightarrow n'$ is then given by $E_{n \rightarrow n'}^{\text{M,PV}} = E_{n'}^{\text{M,PV}} - E_n^{\text{M,PV}}$. Since the PV energy shifts for a given vibrational level n of the M and P enantiomers are related through $E_n^{\text{M,PV}} = -E_n^{\text{P,PV}}$ (Figure 2), the difference between the respective transition energies is

$$\Delta E_{n \rightarrow n'}^{\text{PV}} = E_{n \rightarrow n'}^{\text{M,PV}} - E_{n \rightarrow n'}^{\text{P,PV}} = 2E_{n \rightarrow n'}^{\text{M,PV}}. \quad (3)$$

This energy difference is presented in terms of PV frequency shift by $\Delta\nu_{n \rightarrow n'}^{\text{PV}} = \Delta E_{n \rightarrow n'}^{\text{PV}}/h$, where h is the Planck constant. The frequency shift divided by transition frequency (ν) from harmonic frequency analysis ($\Delta\nu_{n \rightarrow n'}^{\text{PV}}/\nu$) is an important theoretical predictor for the viability of measurement of PV in the corresponding transition.

B. PV in NMR shielding constants

We also analyzed the effect of parity violation on the NMR shieldings in the three molecules. The nuclear spin-dependent (NSD) PV contributions to the four-component (4C) NMR shielding tensors can be expressed in terms of linear response functions, which, for the M and P enantiomers of a chiral molecule, can be written as^{57–59}

$$\langle \sigma_A^{\text{M/P,PV}} \rangle = \frac{G_F m_p}{2\sqrt{2} \hbar c} \frac{\kappa_A}{g_A} \langle \langle \rho_A(\vec{r}) c \vec{\alpha}; \vec{r}_{\text{GO}} \times c \vec{\alpha} \rangle \rangle^{\text{M/P}}, \quad (4)$$

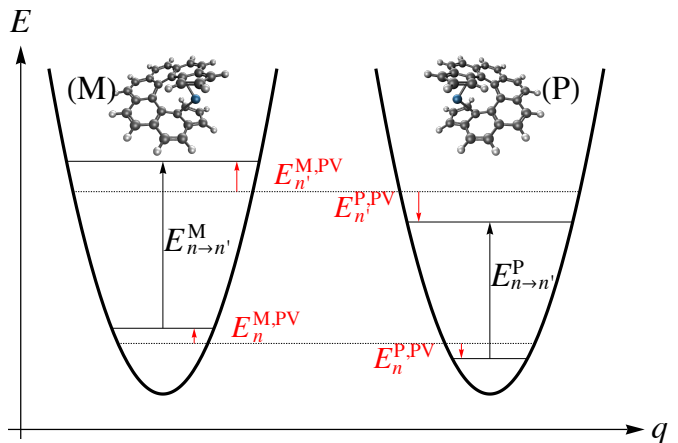


Figure 2. Minus (M) and plus (P) enantiomers of helical osmocene and corresponding PV contributions to the vibrational transitions.

where we have defined $\kappa_A = -2\lambda_A(1 - 4\sin^2\theta_W)$, with λ_A being a nuclear state-dependent parameter that we set to unity in our calculations to facilitate comparison with previous works.^{57,58,60,61} In addition, m_p is the proton mass, $\hbar = h/(2\pi)$ is the reduced Planck constant, c is the speed of light in vacuum, $\vec{\alpha} = (\alpha^1, \alpha^2, \alpha^3)$ is the vector of 4×4 Dirac matrices (with $\alpha^i = \gamma^0\gamma^i$ for $i = 1, 2, 3$), g_A is the nuclear g -factor of nucleus A , and $\vec{r}_{\text{GO}} = \vec{r} - \vec{R}_{\text{GO}}$ is the electron's position operator relative to a fixed gauge origin (GO) for the external magnetic potential.

When the two enantiomers (M and P) of a chiral molecule are analyzed, a difference will appear between the isotropic absolute shielding constants $\sigma_{A,\text{iso}}^{\text{M/P}} = \frac{1}{3}\text{Tr}(\langle \sigma_A^{\text{M/P}} \rangle)$ of the same nucleus A in the two enantiomers. In analogy to Eq. (3), this difference will be given by⁶¹

$$|\Delta\sigma_{A,\text{iso}}| = |\Delta\sigma_{A,\text{iso}}^{\text{PV}}| = |\sigma_{A,\text{iso}}^{\text{M,PV}} - \sigma_{A,\text{iso}}^{\text{P,PV}}| = 2|\sigma_{A,\text{iso}}^{\text{M,PV}}|. \quad (5)$$

Therefore, the measurable absolute value of the NMR frequency splitting of nucleus A , $\Delta\nu_A^{\text{PV-NMR}}$, in a static and homogeneous magnetic field of flux density B_0 is given by

$$|\Delta\nu_A^{\text{PV-NMR}}| = B_0 \frac{e}{4\pi m_p} |g_A \Delta\sigma_{A,\text{iso}}|, \quad (6)$$

where e is the elementary charge.

The values of the diagonal tensor elements of $\langle \sigma_A^{\text{PV}} \rangle$ were computed using the DIRAC23 program package^{53,62}, employing the Dirac–Coulomb Hamiltonian. Given the computational demands of calculating the relativistic 4C linear response functions of Eq. (4), especially in large systems such as those studied in this work, the $\sigma_{A,\text{iso}}^{\text{M/P,PV}}$ constants can only be calculated using small basis sets. Although this restriction does not

allow a highly accurate study of the property, these calculations do provide a reliable estimate of the expected order of magnitude of the effect.^{60,61} In particular, the dyall.aae2z basis sets were used for Fe, Ru, and Os,^{51,63,64} while the 3-21G basis sets were used for C and H.⁶⁵ Furthermore, the common gauge origin (CGO) prescription was applied, with the gauge origin of the external magnetic potential located at the molecular center of mass. The linear response functions were calculated at the random phase approximation (RPA) level of theory, employing DFT wavefunctions. In this way, electron correlation effects were taken into account. In particular, the hybrid functional PBE0⁶⁶ was used, since it provides results in good agreement with experimental nuclear spin-rotation constants, a property closely related to NMR shieldings.^{60,61,67,68}

III. EXPERIMENTAL CONSIDERATIONS

A. Chemical synthesis

The preparation of the heavier ruthenium and osmium homologues of the helical ferrocene (see Figure 1) should be practically feasible by: (i) reproducing the synthesis of the helical ligand as described in the literature;^{35,36} (ii) proceeding with enantiomeric resolution using classical chiral high-performance liquid chromatography (HPLC) techniques; (iii) incorporating heavy metal centers, Ru(II) or Os(II), through efficient synthetic methodologies.⁶⁹⁻⁷¹ Besides synthetic feasibility, the chemical stability of such compounds is unknown and will need to be examined in detail, especially upon heating to bring it into the gas phase for the ultrahigh-resolution spectroscopic studies. Furthermore, the potential high toxicity of the possibly volatile osmium derivatives requires proper precautions.

B. Ultra-precise mid-infrared spectroscopy of cold chiral molecules

For measuring PV vibrational frequency differences between enantiomers, we envision at LPL a state-of-the-art, precise spectroscopy instrument based on the latest advances in cold-molecule research and frequency metrology. We will make a slow, cold beam of the organometallic molecules by producing them inside a buffer gas cell cooled to ~ 1 K. This will provide the low temperature, low speed, and high intensity needed for measuring PV. We have already developed the methods needed to bring into the gas-phase and buffer-gas cool other organometallic species to a few kelvins.^{29,38,72-74} The molecular beam will be probed in a Ramsey interferometer⁷⁵ based on frequency-stabilized metrology-grade lasers calibrated to the cesium fountain clocks of Laboratoire Temps Espace (LTE, the French time-frequency national metrology institute), which realize the standard of frequency of the

international system of units. This machine will be sensitive enough to measure tiny changes in the vibrational frequency, and we project a 10^{-15} relative sensitivity (< 100 mHz) on the frequency difference,²⁹ a two-orders-of-magnitude improvement over the CHFClBr measurement.

When selecting vibrational modes for measurements, a number of experimental considerations have to be taken into account: both the magnitude of the PV frequency shifts and the intensity of the selected mode should be high enough to make the measurement feasible, and their frequencies should be accessible to metrology-grade laser technologies. At LPL, we have developed a method to stabilize mid-infrared lasers to an ultra-stable near-infrared optical frequency comb (OFC) referenced to primary frequency standards of LTE *via* the REFIMEVE optical-fibre infrastructure^{76,77}. Key aspects of the setup that require, in particular, non-linear mixing of the mid-infrared and the comb radiation in a crystal of AgGaSe₂ are briefly presented in the ESI.[†] This approach offers unparalleled sub-Hz frequency accuracies, stabilities, and laser line widths necessary for measuring the tiniest PV frequency differences. We have demonstrated this technology in the 1000 cm^{-1} spectral window first using CO₂ lasers⁷⁸ and then quantum cascade lasers (QCLs)⁷⁹⁻⁸². The CO₂ lasers, until recently one of the very few available ultra-stable sources for precise mid-infrared spectroscopy, span only small portions of the $810\text{--}1120\text{ cm}^{-1}$ range. Mid-infrared QCLs, on the other hand, are commercially available in the $800\text{--}2000\text{ cm}^{-1}$ range and available more sporadically down to $\sim 550\text{ cm}^{-1}$.

We have thus recently started to extend the spectral coverage of our metrology-grade QCLs/OFC system, specifically targeting the $550\text{--}600\text{ cm}^{-1}$ and $1500\text{--}1600\text{ cm}^{-1}$ regions, which, together with the 1000 cm^{-1} window, host the most promising normal modes of the helical osmocene (see below). We have evaluated the spectral performance of the world's first $\sim 580\text{ cm}^{-1}$ continuous-wave distributed feedback (DFB) QCL and demonstrated the first absorption spectroscopy at this wavelength using a QCL.^{83,84} We have even more recently acquired a 1560 cm^{-1} QCL and carried out preliminary investigations of its frequency noise and emission line width, which we report in ESI.[†] Our current setup's spectral coverage is limited to the $850\text{--}1200\text{ cm}^{-1}$ by the combination of the non-linear AgGaSe₂ crystal used and OFC emission spectrum. Frequency stabilizing QCLs at $550\text{--}600\text{ cm}^{-1}$ and $1500\text{--}1600\text{ cm}^{-1}$ requires to determine new such combinations. We have thus carried out simulations of the non-linear mixing efficiency between the OFC and QCLs at our target wavelengths in a panel of birefringent and orientation-patterned (OP) crystals, testing both sum- or difference-frequency-generation (SFG or DFG) as the non-linear phenomenon, in order to identify options which maximize non-linear mixing efficiency. Details of this theoretical study are given in the ESI.[†] Our investigations indicate SFG in GaSe crystals as the solution of choice at both 580 cm^{-1} and 1560 cm^{-1} . If

Table I. Calculated wavenumbers, intensities, PV frequency shifts, and total metal-carbon displacement for selected normal modes in helical osmocene promising for PV measurements. Modes of interest in the currently available sub-Hz metrology-grade laser window are given in bold font. *Mode 108 is listed for comparison in Figures 6–9 and the corresponding discussion below.

Mode number	$\tilde{\nu}$ (cm ⁻¹)	Intensity (km/mol)	$\Delta\nu_{0\rightarrow 1}^{\text{PV}}$ (Hz)	$\Delta\nu_{0\rightarrow 1}^{\text{PV}}/\nu$	d_{MC} (Å)
30	586.5	28.89	1.03	5.84×10^{-14}	0.80
31	595.9	3.55	-5.77	-3.23×10^{-13}	1.25
32	602.3	1.18	6.85	3.79×10^{-13}	1.46
35	636.0	0.81	2.64	1.38×10^{-13}	0.75
36	641.5	7.82	-3.27	-1.70×10^{-13}	1.44
37	658.3	0.71	-3.04	-1.54×10^{-13}	0.87
40	707.7	0.86	2.46	1.16×10^{-13}	1.08
46	795.0	4.88	2.12	8.89×10^{-14}	0.54
48	824.0	16.58	-0.60	-2.44×10^{-14}	0.34
50	836.9	12.64	0.19	7.46×10^{-15}	0.24
54	859.6	18.37	-1.40	-5.44×10^{-14}	0.77
56	867.0	73.99	0.37	1.41×10^{-14}	0.37
59	891.6	20.07	0.49	1.84×10^{-14}	0.50
61	913.1	4.39	-2.83	-1.03×10^{-13}	0.49
72	1053.7	12.32	-0.63	-2.00×10^{-14}	0.62
94	1391.1	9.87	-0.32	-7.66×10^{-15}	0.94
102	1481.9	5.55	3.82	8.60×10^{-14}	1.33
103	1487.7	8.34	-0.53	-1.19×10^{-14}	1.35
*108	1592.5	5.54	-0.09	1.82×10^{-15}	0.29

cutting the GaSe crystal to the correct phase-matching angle is not possible, SFG in OP-GaAs, OP-GaP and AgGaSe₂ also happen to be reasonable fallback solutions.

The QCLs that will be used in the PV measurements typically cover a few wavenumbers only. As will be shown in the following, the size of the PV vibrational shift can vary by a few orders of magnitude depending on the vibrational mode. Theoretical guidance on the optimal vibrational modes for measurements is thus crucial for determining a target frequency range and designing the metrology-grade laser system to be built and tuned at LPL.

IV. RESULTS AND DISCUSSION

A. Optimized geometries

The structure of helical ferrocene has been elucidated by the X-ray diffraction.³⁶ Our optimized structure is in good agreement with experiment, with root mean square deviation (RMSD) of 0.13 Å (see also Figure S1 in ESI[†] for the visual comparison). We expect similar accuracy for the optimized geometries of the two heavier systems, where experimental information is not yet available.

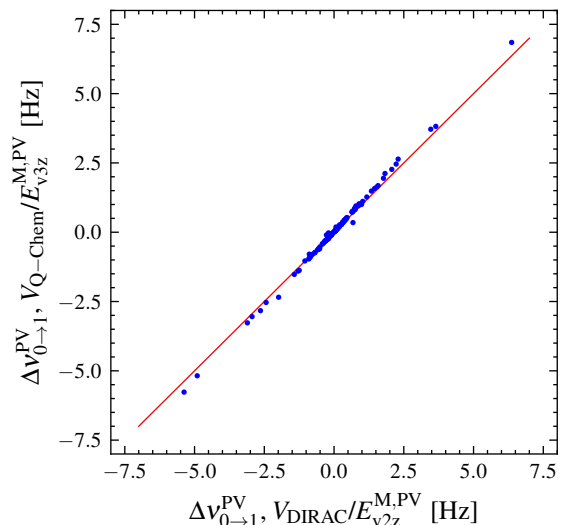


Figure 3. Correlation between PV frequency shifts in helical osmocene calculated on two different levels of theory – the higher level uses dyall.v3z basis set for Os in the $E^{\text{M,PV}}$ calculations and potential $V(q)$ calculated in Q-Chem; the lower level uses dyall.v2z basis set for Os in the $E^{\text{M,PV}}$ calculations and potential $V(q)$ from the same DIRAC calculations. In both cases, the v2z basis set was used for the carbons and the hydrogens. Red line shows the ideal linear correlation.

B. PV in vibrational transitions

Table I presents a selection of recommended vibrational modes of helical osmocene for potential PV measurements (Table S1 in ESI[†] contains all calculated vibrational modes). These modes were selected based on their frequency falling within the desired laser frequency range (500–2000 cm⁻¹) and on having exceptionally high intensity and/or high PV frequency shift. All these modes have a relative PV frequency shift $\Delta\nu_{\text{PV}}/\nu$ of $\sim 10^{-14}$ or more. This is a level of frequency sensitivity already demonstrated at LPL^{19,75} and at least an order of magnitude larger than the 10^{-15} sensitivity aimed for in the new experiment. It can be compared to the predicted -8×10^{-17} relative PV shift of CHFCIBr^{22–26} on which much of the experimental work has been conducted so far. Normal modes 56, 59, 61 and 72 are in the laser window with currently available sub-Hz metrology-grade sources at LPL, are reasonably infrared active, and have a predicted relative PV shift on the 10^{-14} level or more. Vibrational modes 56 and 61 look particularly promising, the former given its remarkably high intensity (the highest intensity transition in the entire spectrum), the latter given its very large predicted $\sim 10^{-13}$ relative PV shift. Importantly, this is twice higher than the most sensitive transition of Os(acac)₃ reported in our previous study³⁸ in the 1000 cm⁻¹ region where our sub-Hz laser technology is currently available. Table I also lists a series of vibrational modes exhibiting relative PV shifts rang-

ing from $\sim 10^{-14}$ to a few 10^{-13} and reasonable intensities in the 600 cm^{-1} and 1500 cm^{-1} spectral windows in which metrology-grade laser systems are currently being developed at LPL. Vibrational modes 30 and 32 are especially favorable, not only because they exhibit respectively a particularly intense transition and the highest predicted relative PV shift in the entire spectrum – about 4×10^{-13} – but also because of their lower 600 cm^{-1} frequencies, which may prevent the onset of intramolecular vibrational energy redistribution that could obscure the spectra at higher frequencies.

In order to assess the robustness of the predicted relative PV shifts with respect to the computational parameters, we have carried out additional calculations. In Figure 3, we compare PV shifts of all calculated modes at the production level of theory using the `dyall.v3z` basis set⁵¹ for Os to a lower-level calculation using a more modest `dyall.v2z` basis set⁵² as well as potential energy curves from the DIRAC calculation instead of the original Q-chem potentials, consistent with the harmonic frequency analysis. We found the obtained vibrational frequency shifts in excellent agreement with the higher-level calculations, indicating that this lower-cost approach (at least twice as fast) can be used as a predictor in future work. Furthermore, we have investigated the effect of different DFT functionals on the calculated PV frequency shifts and found the results to be in good agreement for the CAMB3LYP*⁵⁰, CAMB3LYP*(EFG)⁸⁵, B3LYP^{86–89}, PBE⁹⁰, LDA^{88,91} functionals, and for Hartree–Fock calculations, as shown in Figure 4, confirming the robustness of our predictions. The complete list of the calculated PV contributions for these modes can be found in Table S3 in ESI.[†] Note that functionals CAMB3LYP, CAMB3LYP* and CAMB3LYP*(EFG) differ in their attenuation parameters which are optimized, respectively, for energy calculations ($\alpha=0.19$, $\beta=0.46$, and $\mu=0.33$), PV calculations ($\alpha=0.2$, $\beta=0.12$, and $\mu=0.9$), and electric field gradient (EFG) calculations ($\alpha=0.4$, $\beta=0.179$, and $\mu=0.99$).

Our previous study on $\text{Ru}(\text{acac})_3$ ³⁸ identified a positive correlation between the size of the PV frequency shift for a specific vibration and the total ligand displacement along the vibration motion. Here, we perform a similar analysis, defining the metal-carbon displacement as

$$d_{\text{MC}} = \sum_{i=1}^{10} \sqrt{(\Delta x_{\text{MC},i})^2 + (\Delta y_{\text{MC},i})^2 + (\Delta z_{\text{MC},i})^2}, \quad (7)$$

where the summation runs over the 10 neighboring cyclopentadienyl carbon atoms (see Figure 1) and $\Delta\alpha_{\text{MC},i}$ ($\alpha = x, y, z$) represent the relative displacements of the involved metal and carbon atoms. The PV frequency shifts and the ligand displacements for all calculated vibrational modes of helical osmocene are given in Table S1 in ESI.[†] The calculated absolute PV shifts are plotted against the total ligand displacement of the corresponding transition in Figure 5. We observe that small ligand displacements with respect to the metal consistently yield relatively low PV frequency shifts. However,

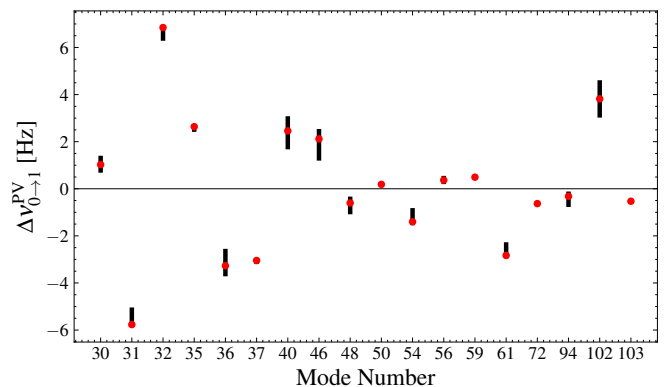


Figure 4. PV Frequency shifts of the recommended modes calculated using different DFT functionals and Hartree–Fock. Red dots represent the CAM-B3LYP* values, while black bars represent the range of frequency shifts calculated using all methods (based on the values in Table S3 in ESI[†]).

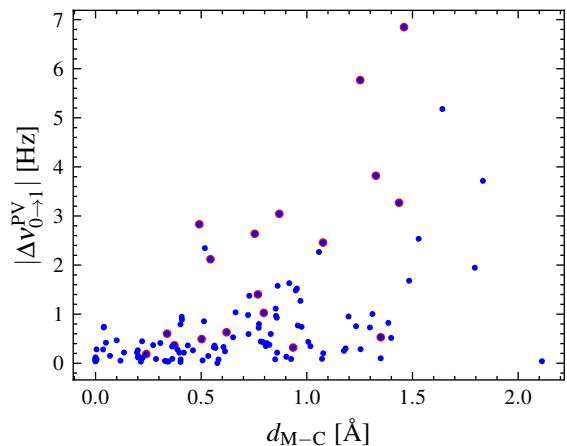


Figure 5. Absolute values of the PV frequency shifts of the vibrational transitions of helical osmocene plotted against the total metal-carbon displacement. The vibrations selected as promising for measurements (see Table I) are marked in red.

conversely, large ligand displacements do not necessarily lead to a high PV frequency shift, making the displacement a predictor with limited applicability for this class of molecules.

To aid our discussion further, we consider three representative vibrational modes with frequencies within the range of commercially available lasers currently considered at LPL and with a relatively high intensity. These are mode 102 (cyclopentadienyl symmetric breathing), mode 103 (cyclopentadienyl asymmetric breathing), and mode 108 (side ring deformation). Modes 102 and 103 form a symmetric pair, in which mode 102 exhibits a significantly higher PV shift compared to mode 103. While modes 102 and 103 both have very large ligand displacements (1.33 Å and 1.35 Å, respectively), mode 108 with

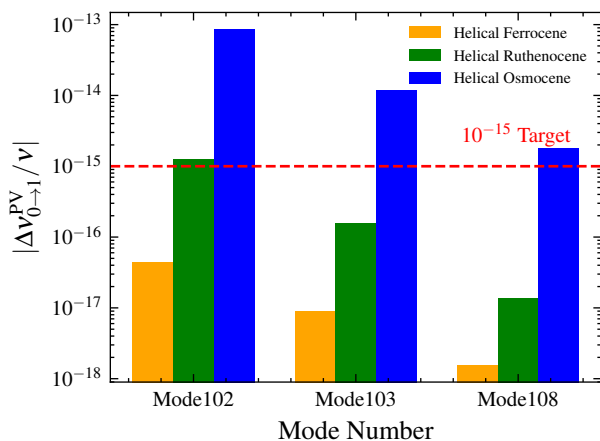


Figure 6. Relative PV frequency shifts of vibrational modes 102, 103, and 108 for helical ferrocene, helical ruthenocene, and helical osmocene.

its relatively small ligand displacement (0.29 Å) is selected for contrast.

Figure 6 shows the magnitude of relative PV frequency shifts for the three selected vibrational modes in helical ferrocene, ruthenocene, and osmocene. The structure and properties of the three systems are expected to be similar, and thus the same modes were selected in each molecule. Of the three systems, only the heaviest, helical osmocene, has relative PV frequency shifts that surpass the projected detection limit of 10^{-15} on all three modes, motivating us to focus further on this molecule. As expected from the small ligand displacement, mode 108 yields a small PV frequency shift (−0.09 Hz). In contrast, mode 102, with the highest PV frequency shift (3.83 Hz) in the 1000 cm^{-1} spectral window currently accessible at LPL, has a seven times higher PV shift than mode 103 (−0.53 Hz), despite a similar magnitude of ligand displacement. It is thus clear that other factors besides the ligand displacement play a role in determining the size of the PV frequency shift.

Figure 7 shows the potential energy curves and the PV energy curves for the three vibrational modes discussed above. While the potential energy curves are almost ideally harmonic and very similar for all three modes, the shapes of the parity-violating energy curves are markedly different. Furthermore, based on the analytic perturbative contribution analysis in ESI[†] Table S1, PV shifts of these three modes are dominated by the curvature term of PV curve with the anharmonic term being negligible. In agreement with the ligand displacement analysis, the PV curve of mode 108 is almost flat and close to zero. However, while the magnitude of the ligand displacement for modes 102 and 103 (which form an antisymmetric pair) is almost identical, mode 102 has a significantly larger PV response compared to mode 103, leading to a significantly higher PV frequency shift. This observation is in line with the relatively poor correlation between PV

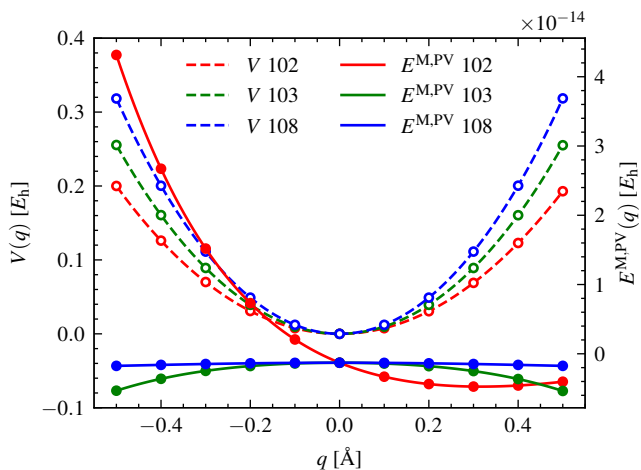


Figure 7. PV energy curves (solid lines, filled circles) and potential energy curves (dashed lines, empty circles) for vibrational modes 102, 103, and 108 in helical osmocene.

shift and atom displacement in Figure 5.

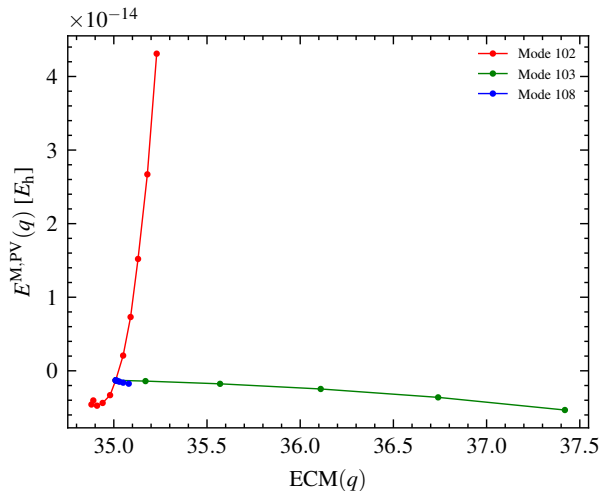


Figure 8. $E^{M,PV}$ vs ECM for vibrational modes 102, 103, and 108 in helical osmocene. Modes 103 and 108 are symmetric, and thus the positively and negatively displaced points are overlaid, resulting in seemingly fewer data points.

We have analyzed vibrational modes 102, 103, and 108 using the electronic chirality measure (ECM)⁹² obtained using the PyECM software.⁹³ ECM is a descriptor based on the electronic density that quantifies the chirality degree of a molecule.⁹² It was shown that for some organic molecules, such as alanine and glyceraldehyde, there is a correlation between $E^{M,PV}$ and ECM.⁹⁴ Figure 8 shows the relationship between the total PV energy and the value of ECM along the displacement coordinate for the three selected vibrational modes. In general, we observe a correlation between the ECM and the $E^{M,PV}$ values

within each mode. However, the behavior for each of the studied modes is vastly different. For mode 108, the minimal change in the ECM is consistent with the very small change in $E^{\text{M,PV}}$ along the displacement. On the other hand, the relationships between the ECM and $E^{\text{M,PV}}$ values in modes 102 and 103 are markedly different. While mode 102 displays a big change in $E^{\text{M,PV}}$, the corresponding ECM values remain within a very tight range. In contrast, the large ECM variation along mode 103 accompanies a rather small $E^{\text{M,PV}}$ change. For the three modes, the higher magnitude for $E^{\text{M,PV}}$ is obtained within the range of higher ECM. Furthermore, ECM values are by definition unsigned, and hence the changes of sign commonly observed for $E^{\text{M,PV}}$ values (as seen, e.g., in mode 102) cannot be directly reproduced. From this behavior, it can be concluded that the ECM analysis in this system does not allow for the prediction of which mode will present the higher relative PV frequency shift.

In a further attempt to interpret the results, we employed chirality density analysis^{31,95} and orbital projection analysis,^{96,97} details of which can be found in ESI[†] Section S5. Chirality density plots (Figures S3 and S4 in ESI[†]) reveal that significant changes in chiral density along the vibrational coordinate q occur at the Os nucleus in mode 102, leading to a strong PV response, while in modes 103 and 108 these changes are smaller and located mostly outside of the Os nucleus and penetrating it only partially, leading to relatively flat $E^{\text{M,PV}}$ curves. The atomic orbital projection analysis^{96,97} shows that the PV curve qualitatively follows the largest osmium ($6s|5p_{1/2}$) contribution (compare Figures 7 and 9). In ESI[†] Section S5.3, we discuss the details of the projection analysis and complications due to the significant influence of molecular polarization effects.

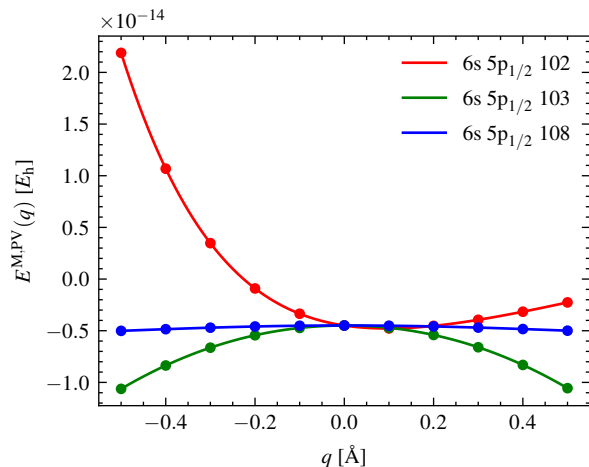


Figure 9. Osmium intraatomic $\langle 6s|5p_{1/2} \rangle$ contributions to PV energy curves for vibrational modes 102, 103, and 108 in helical osmocene.

C. PV effects in NMR shielding constants

To further characterize the behavior of PV effects in the three molecules investigated in this work, we also evaluated their contributions to NMR shielding constants. At a magnetic flux density of $B_0 = 20$ T, as considered in recent experimental proposals for searches of PV effects on NMR parameters,⁹⁸ the predicted NMR frequency splittings range from about 0.02 mHz for Fe in ferrocene to about 0.8 mHz for Os in osmocene (see Table II). For helical osmocene, this value lies within roughly one order of magnitude of the projected experimental sensitivity. Although still challenging, this suggests that the system may be of interest for PV searches also in the NMR context and could motivate further studies using other spectroscopic approaches.

Table II. Calculated values of $2|g_A \sigma_{A,\text{iso}}^{\text{M,PV}}|$ in parts per trillion (ppt) and $|\Delta\nu_A^{\text{PV-NMR}}|$ (for $B_0 = 20$ T, in mHz) for the A nuclei (with $A = \text{Fe, Ru, and Os}$) in the helicene series of molecules.

A	$2 g_A \sigma_{A,\text{iso}}^{\text{M,PV}} / \text{ppt}$	$ \Delta\nu_A^{\text{PV-NMR}}(20 \text{ T}) / \text{mHz}$
⁵⁷ Fe	0.11	0.02
¹⁰¹ Ru	0.59	0.09
¹⁸⁹ Os	5.38	0.82

V. CONCLUSIONS

We have calculated the PV vibrational frequency shifts for a selection of normal modes in helical osmocene, a highly promising candidate species for the first detection of parity violation in molecules. This molecule is the first system with inherent helical chirality investigated in the context of PV searches. We have pinpointed a number of mid-infrared transitions which fall in accessible laser windows and exhibit exceptionally large PV shifts of hundreds of millihertz to ~ 7 Hz. This pushes the $|\Delta\nu_{\text{PV}}/\nu|$ of these modes into the $\sim 10^{-13}$ regime, exceeding by up to 2 orders of magnitude the projected instrumental sensitivity of the ultrahigh-resolution experiment being built at LPL.

The effect of computational setting on the calculated PV energy shifts was investigated, and a lower-cost theoretical approach was identified for future studies. The results were also found to be robust with respect to the used DFT functional. A variety of proposed structural and electronic predictors of PV effects were tested. In this class of systems, we found their applicability to be limited, motivating the use of explicit calculations based on low-cost computational methods.

We have also investigated the size of the PV effects in NMR shielding constants. For helical osmocene, these were found to be just an order of magnitude below the

projected sensitivity of planned experimental searches for PV in NMR spectroscopy.

The predicted large PV effects in helical osmocene provide a strong motivation to synthesize this compound and to bring it into the gas phase. A strategy for synthesizing helical osmocene has been proposed. Once synthesized, its enantiomeric resolution and stability upon heating to bring it into the gas phase for the ultrahigh-resolution spectroscopic studies will be investigated.

ACKNOWLEDGMENTS

The authors thank the Center for Information Technology of the University of Groningen for their support and for providing access to the Hábrók high-performance computing cluster. Eduardus wishes to acknowledge the Indonesia Endowment Fund for Education/*Lembaga Pengelola Dana Pendidikan* (LPDP) for research funding. LFP acknowledges the support from the project number VIC.212.016 of the talent programme VICI, financed by the Dutch Research Council (NWO), and support from the Scientific Grant Agency of the Slovak Republic (project 1/0254/24). IAA acknowledges partial support from FONCYT through grants PICT-2021-I-A-0933 and PICT-2020-SerieA-0052, and CONICET through grant PIBAA-2022-0125CO. JJA acknowledges the Institute for Modelling and Innovative Technologies (IMIT, CONICET) and the National University of the Northeast (UNNE) for support and access to the IMIT high-performance computing cluster. The work of IAA and AB was supported by the project *Probing Particle Physics with Polyatomic molecules* with project number OCENW.M.21.098 of the research programme M2, which is financed by the Dutch Research Council (NWO). The work of ABo, MM and BD was supported by the Agence Nationale de la Recherche projects Ultimos (Grant No. ANR-24-CE30-2959-01); CNRS; Université Sorbonne Paris Nord; and was part of 23FUN04 COMOMET that has received funding from the European Partnership on Metrology, co-financed by the European Union's Horizon Europe Research and Innovation Programme and from by the Participating States, funder ID: 10.13039/100019599. ABo, MM, and BD thank Anne Amy-Klein for the first SFG calculations based on AgGaSe₂, preliminary modeling of OP non-linear crystals, and Anne Amy-Klein, Christof Janssen, and Laurent Hilico for many fruitful discussions. In memory of Jean-Jacques Zondy.

REFERENCES

- S. Mason, "Biomolecular homochirality," *Chemical Society Reviews* **17**, 347–359 (1988).
- W. A. Bonner, "Chirality and life," *Origins of Life and Evolution of the Biosphere* **25**, 175–190 (1995).
- D. G. Blackmond, "Autocatalytic models for the origin of biological homochirality," *Chemical Reviews* **120**, 4831–4847 (2020).
- R. F. Martínez, L. A. Cuccia, C. Viedma, and P. Cintas, "On the origin of sugar handedness: Facts, hypotheses and missing links—a review," *Origins of Life and Evolution of Biospheres* **52**, 21–56 (2022).
- Q. Sallembien, L. Bouteiller, J. Crassous, and M. Raynal, "Possible chemical and physical scenarios towards biological homochirality," *Chemical Society Reviews* **51**, 3436–3476 (2022).
- Y. Yamagata, "A hypothesis for the asymmetric appearance of biomolecules on earth," *Journal of Theoretical Biology* **11**, 495–498 (1966).
- S. F. Mason, "Origins of biomolecular handedness," *Nature* **311**, 19–23 (1984).
- G. E. Tranter, "Parity-violating energy differences of chiral minerals and the origin of biomolecular homochirality," *Nature* **318**, 172–173 (1985).
- M. Quack, "How important is parity violation for molecular and biomolecular chirality?" *Angewandte Chemie International Edition* **41**, 4618–4630 (2002).
- R. Wesendrup, J. K. Laerdahl, R. N. Compton, and P. Schwerdtfeger, "Biomolecular Homochirality and Electroweak Interactions. I. The Yamagata Hypothesis," *The Journal of Physical Chemistry A* **107**, 6668–6673 (2003).
- D. W. Rein, "Some remarks on parity violating effects of intramolecular interactions," *Journal of Molecular Evolution* **4**, 15–22 (1974).
- V. Letokhov, "On difference of energy levels of left and right molecules due to weak interactions," *Physics Letters A* **53**, 275–276 (1975).
- C. S. Wu, E. Ambler, R. W. Hayward, D. D. Hoppes, and R. P. Hudson, "Experimental test of parity conservation in beta decay," *Phys. Rev.* **105**, 1413–1415 (1957).
- M.-A. Bouchiat, "Atomic Parity Violation. Early days, present results, prospects," *Nuovo Cimento C* **35**, 78–84 (2012), arXiv:1111.2172 [physics.atom-ph].
- M. S. Safronova, D. Budker, D. DeMille, D. F. J. Kimball, A. Derevianko, and C. W. Clark, "Search for new physics with atoms and molecules," *Reviews of Modern Physics* **90**, 025008 (2018).
- C. Daussy, T. Marrel, A. Amy-Klein, C. T. Nguyen, C. J. Bordé, and C. Chardonnet, "Limit on the parity nonconserving energy difference between the enantiomers of a chiral molecule by laser spectroscopy," *Physical Review Letters* **83**, 1554–1557 (1999).
- J. Crassous, J.-P. Monier, F. Dutasta, M. Ziskind, C. Daussy, C. Grain, and C. Chardonnet, "Search for resolution of chiral fluorohalogenomethanes and parity violation effects at the molecular level," *ChemPhysChem* **4**, 541 (2003).
- J. Crassous, C. Chardonnet, T. Saue, and P. Schwerdtfeger, "Recent experimental and theoretical developments towards the observation of parity violation (pv) effects in molecules by spectroscopy," *Organic and Biomolecular Chemistry* **3**, 2218–2224 (2005).
- B. Darquié, C. Stoeffler, S. Zrig, J. Crassous, P. Soulard, P. Asselin, T. R. Huet, L. Guy, R. Bast, T. Saue, P. Schwerdtfeger, A. Shelkovich, C. Daussy, A. Amy-Klein, and C. Chardonnet, "Progress toward the first observation of parity violation in chiral molecules by high-resolution laser spectroscopy," *Chirality* **22**, 870–884 (2010).
- M. Quack, G. Seyfang, and G. Wichmann, "Perspectives on parity violation in chiral molecules: theory, spectroscopic experiment and biomolecular homochirality," *Chemical Science* **13**, 10598–10643 (2022).
- M. Ziskind, C. Daussy, T. Marrel, and C. Chardonnet, "Improved sensitivity in the search for a parity-violating energy difference in the vibrational spectrum of the enantiomers of CHFClBr," *The European Physical Journal D - Atomic, Molecular, Optical and Plasma Physics* **20**, 219–225 (2002).
- M. Quack and J. Stohner, "Influence of parity violating weak nuclear potentials on vibrational and rotational frequencies in chiral molecules," *Physical Review Letters* **84**, 3807–3810 (2000).

- ²³P. Schwerdtfeger, T. Saue, J. N. P. van Stralen, and L. Visscher, "Relativistic second-order many-body and density-functional theory for the parity-violation contribution to the C-F stretching mode in chfclbr," *Physical Review A* **71**, 012103 (2005).
- ²⁴C. Thierfelder, G. Rauhut, and P. Schwerdtfeger, "Relativistic coupled-cluster study of the parity-violation energy shift of CHFClBr," *Physical Review A* **81**, 032513 (2010).
- ²⁵G. Rauhut and P. Schwerdtfeger, "Parity-violation effects in the vibrational spectra of CHFClBr and CDFClBr," *Physical Review A* **103**, 042819 (2021).
- ²⁶S. A. Brück, N. Sahu, K. Gaul, and R. Berger, "Quasi-relativistic approach to analytical gradients of parity violating potentials," *The Journal of Chemical Physics* **158**, 194109 (2023).
- ²⁷N. Saleh, S. Zrig, T. Roisnel, L. Guy, R. Bast, T. Saue, B. Darquié, and J. Crassous, "A chiral rhenium complex with predicted high parity violation effects: synthesis, stereochemical characterization by VCD spectroscopy and quantum chemical calculations." *Physical chemistry chemical physics : PCCP* **15**, 10952–9 (2013).
- ²⁸N. Saleh, R. Bast, N. Vanthuyne, C. Roussel, T. Saue, B. Darquié, and J. Crassous, "An oxorhenium complex bearing a chiral cyclohexane-1-olato-2-thiolato ligand: Synthesis, stereochemistry, and theoretical study of parity violation vibrational frequency shifts," *Chirality* **30**, 147–156 (2018), arXiv: 1803.02770.
- ²⁹A. Cournol, M. Manceau, M. Pierens, L. Lecordier, D. Tran, R. Santagata, B. Argece, A. Goncharov, O. Lopez, M. Abgrall, Y. Le Coq, R. Le Targat, H. Álvarez Martínez, W. Lee, D. Xu, P.-E. Pottie, R. Hendricks, T. Wall, J. Bieniewska, B. Sauer, M. Tarbutt, A. Amy-Klein, S. Tokunaga, and B. Darquié, "A new experiment to test parity symmetry in cold chiral molecules using vibrational spectroscopy," *Quantum Electronics* **49**, 288 (2019).
- ³⁰B. Y. Zel'Dovich, D. B. Saakyan, and I. I. Sobel'Man, "Energy difference between right-hand and left-hand molecules, due to parity nonconservation in weak interactions of electrons with nuclei," *Soviet Journal of Experimental and Theoretical Physics Letters* **25**, 94 (1977), Available at: http://jetpletters.ru/ps/1388/article_21066.shtml.
- ³¹R. Bast, A. Koers, A. S. P. Gomes, M. Iliáš, L. Visscher, P. Schwerdtfeger, and T. Saue, "Analysis of parity violation in chiral molecules," *Physical Chemistry Chemical Physics* **13**, 864–876 (2011).
- ³²R. Martin and M.-J. Marchant, "Thermal racemisation of [6], [7], [8] and [9] helicene." *Tetrahedron Letters* **13**, 3707 – 3708 (1972).
- ³³R. Martin and M. Marchant, "Thermal racemisation of hepta-, octa-, and nonahelicene: Kinetic results, reaction path and experimental proofs that the racemisation of hexa- and heptahelicene does not involve an intramolecular double diels-alder reaction." *Tetrahedron* **30**, 347–349 (1974).
- ³⁴M. P. Johansson and M. Patzschke, "Fixing the chirality and trapping the transition state of helicene with atomic metal glue," *Chemistry-A European Journal* **15**, 13210–13218 (2009).
- ³⁵T. J. Katz and J. Pesti, "The synthesis of a helical ferrocene," *Journal of the American Chemical Society* **104**, 346–347 (1982).
- ³⁶J. C. Dewan, "Structural characterization of the helical ferrocene (.+.-)-[(1,2,3,3a,13a,14,15,16,16a,16f-.eta.)-diindenol[5,4-c:4',5'-g]phenanthrene]iron," *Organometallics* **2**, 83–88 (1983).
- ³⁷A. Sudhakar and T. J. Katz, "Asymmetric synthesis of helical metallocenes," *Journal of the American Chemical Society* **108**, 179–181 (1986).
- ³⁸M. R. Fiechter, P. A. B. Haase, N. Saleh, P. Souldard, B. Tremblay, R. W. A. Havenith, R. G. E. Timmermans, P. Schwerdtfeger, J. Crassous, B. Darquié, L. F. Pašteka, and A. Borschevsky, "Toward Detection of the Molecular Parity Violation in Chiral Ru(acac)₃ and Os(acac)₃," *The Journal of Physical Chemistry Letters* **13**, 10011–10017 (2022), pMID: 36264147.
- ³⁹E. Epifanovsky, A. T. B. Gilbert, X. Feng, J. Lee, Y. Mao, N. Mardirossian, *et al.*, "Software for the frontiers of quantum chemistry: An overview of developments in the Q-Chem 5 package," *The Journal of Chemical Physics* **155**, 084801 (2021).
- ⁴⁰N. Mardirossian and M. Head-Gordon, "ωB97M-V: A combinationally optimized, range-separated hybrid, meta-GGA density functional with VV10 nonlocal correlation," *The Journal of Chemical Physics* **144**, 214110 (2016).
- ⁴¹F. Weigend and R. Ahlrichs, "Balanced basis sets of split valence, triple zeta valence and quadruple zeta valence quality for H to Rn: Design and assessment of accuracy," *Physical Chemistry Chemical Physics* **7**, 3297–3305 (2005).
- ⁴²D. Andrae, U. Häußermann, M. Dolg, H. Stoll, and H. Preuß, "Energy-adjusted ab initio pseudopotentials for the second and third row transition elements," *Theoretica chimica acta* **77**, 123–141 (1990).
- ⁴³R. Berger, "Chapter 4 - parity-violation effects in molecules," in *Relativistic Electronic Structure Theory*, Theoretical and Computational Chemistry, Vol. 14, edited by P. Schwerdtfeger (Elsevier, 2004) pp. 188–288.
- ⁴⁴L. Montanet, K. Gieselmann, R. M. Barnett, D. E. Groom, T. G. Trippe, *et al.* (Particle Data Group), "Review of particle properties," *Physical Review D* **50**, 1173–1814 (1994).
- ⁴⁵(), DIRAC, a relativistic ab initio electronic structure program, Release DIRAC19 (2019), written by A. S. P. Gomes, T. Saue, L. Visscher, H. J. Aa. Jensen, and R. Bast, with contributions from I. A. Aucar, V. Bakken, K. G. Dyall, S. Dubillard, U. Ekström, E. Eliav, T. Enevoldsen, E. Faßhauer, T. Fleig, O. Fossgaard, L. Halbert, E. D. Hedegård, B. Heimlich-Paris, T. Helgaker, J. Henriksson, M. Iliáš, Ch. R. Jacob, S. Knecht, S. Komorovský, O. Kullie, J. K. Lærdahl, C. V. Larsen, Y. S. Lee, H. S. Nataraj, M. K. Nayak, P. Norman, G. Olejniczak, J. Olsen, J. M. H. Olsen, Y. C. Park, J. K. Pedersen, M. Pernpointner, R. di Remigio, K. Ruud, P. Sałek, B. Schimmelpennig, B. Senjean, A. Shee, J. Sikkema, A. J. Thorvaldsen, J. Thyssen, J. van Stralen, M. L. Vidal, S. Villaume, O. Visser, T. Winther, and S. Yamamoto (available at <http://dx.doi.org/10.5281/zenodo.3572669>, see also <http://www.diracprogram.org>).
- ⁴⁶H. Hellmann, *Einführung in die Quantenchemie* (Franz Deuticke, Leipzig und Wien, 1937).
- ⁴⁷R. P. Feynman, "Forces in molecules," *Physical Review* **56**, 340–343 (1939).
- ⁴⁸B. A. Heß, C. M. Marian, U. Wahlgren, and O. Gropen, "A mean-field spin-orbit method applicable to correlated wavefunctions," *Chemical Physics Letters* **251**, 365–371 (1996).
- ⁴⁹B. Schimmelpennig, "AMFI, an atomic mean-field spin-orbit integral program," (1996 and 1999), university of Stockholm.
- ⁵⁰C. Thierfelder, G. Rauhut, and P. Schwerdtfeger, "Relativistic coupled-cluster study of the parity-violation energy shift of CHFClBr," *Physical Review A* **81**, 032513 (2010).
- ⁵¹K. G. Dyall, "Relativistic double-zeta, triple-zeta, and quadruple-zeta basis sets for the 5d elements Hf–Hg," *Theoretical Chemistry Accounts* **112**, 403–409 (2004), revision K.G. Dyall and A.S.P. Gomes, *Theor. Chem. Acc.* **125**, 97–100 (2010).
- ⁵²K. G. Dyall, "Relativistic double-zeta, triple-zeta, and quadruple-zeta basis sets for the light elements H–Ar," *Theoretical Chemistry Accounts* **135**, 128 (2016).
- ⁵³T. Saue, R. Bast, A. S. P. Gomes, H. J. Aa. Jensen, L. Visscher, I. A. Aucar, R. Di Remigio, K. G. Dyall, E. Eliav, E. Faßhauer, *et al.*, "The DIRAC code for relativistic molecular calculations," *The Journal of Chemical Physics* **152**, 204104 (2020).
- ⁵⁴B. V. Noumerov, "A Method of Extrapolation of Perturbations," *Monthly Notices of the Royal Astronomical Society* **84**, 592–602 (1924).
- ⁵⁵J. W. Cooley, "An improved eigenvalue corrector formula for solving the schrodinger equation for central fields," *Mathematics of Computation* (1961), 10.2307/2003025.
- ⁵⁶R. Bast, "Numerov v0.5.0," <https://doi.org/10.5281/zenodo.1000406> (2017).
- ⁵⁷G. Laubender and R. Berger, "Ab Initio Calculation of Parity-Violating Chemical Shifts in NMR Spectra of Chiral Molecules," *ChemPhysChem* **4**, 395–399 (2003).
- ⁵⁸R. Bast, P. Schwerdtfeger, and T. Saue, "Parity Nonconservation Contribution to the Nuclear Magnetic Resonance Shielding

- Constants of Chiral Molecules: A Four-Component Relativistic Study,” *The Journal of Chemical Physics* **125**, 064504 (2006).
- ⁵⁹I. A. Aucar, M. T. Colombo Jofré, and G. A. Aucar, “A relativistic relationship between parity-violating nuclear spin-rotation tensors and parity-violating NMR shielding tensors,” *The Journal of Chemical Physics* **158**, 094306 (2023).
- ⁶⁰I. A. Aucar and A. Borschevsky, “Relativistic Study of Parity-Violating Nuclear Spin-Rotation Tensors,” *The Journal of Chemical Physics* **155**, 134307 (2021).
- ⁶¹I. A. Aucar, Y. Chamorro, and A. Borschevsky, “Parity-Violating Contributions to Nuclear Spin-Rotation Interactions and to NMR Shielding Constants in Tetrahedral Molecules,” *Physical Review A* **106**, 062802 (2022).
- ⁶²(), DIRAC, a relativistic ab initio electronic structure program, Release DIRAC23 (2023), written by R. Bast, A. S. P. Gomes, T. Saue and L. Visscher and H. J. Aa. Jensen, with contributions from I. A. Aucar, V. Bakken, C. Chibueze, J. Creutzberg, K. G. Dyall, S. Dubillard, U. Ekström, E. Eliav, T. Enevoldsen, E. Faßhauer, T. Fleig, O. Fossgaard, L. Halbert, E. D. Hedegård, T. Helgaker, B. Helmich-Paris, J. Henriksson, M. van Horn, M. Iliáš, Ch. R. Jacob, S. Knecht, S. Komorovský, O. Kullie, J. K. Lærdahl, C. V. Larsen, Y. S. Lee, N. H. List, H. S. Nataraj, M. K. Nayak, P. Norman, A. Nyvang, G. Olejniczak, J. Olsen, J. M. H. Olsen, A. Papadopoulos, Y. C. Park, J. K. Pedersen, M. Pernpointner, J. V. Pototschnig, R. di Remigio, M. Repisky, K. Ruud, P. Salek, B. Schimmelpennig, B. Senjean, A. Shee, J. Sikkema, A. Sunaga, A. J. Thorvaldsen, J. Thyssen, J. van Stralen, M. L. Vidal, S. Villaume, O. Visser, T. Winther, S. Yamamoto and X. Yuan (available at <https://doi.org/10.5281/zenodo.7670749>, see also <https://www.diracprogram.org>).
- ⁶³K. G. Dyall and A. S. P. Gomes, Unpublished.
- ⁶⁴K. G. Dyall, “Relativistic double-zeta, triple-zeta, and quadruple-zeta basis sets for the 4d elements Y–Cd,” *Theoretical Chemistry Accounts* **117**, 483–489 (2007), <https://doi.org/10.5281/zenodo.7574628>.
- ⁶⁵J. S. Binkley, J. A. Pople, and W. J. Hehre, “Self-consistent molecular orbital methods. 21. Small split-valence basis sets for first-row elements,” *Journal of the American Chemical Society* **102**, 939–947 (1980).
- ⁶⁶C. Adamo and V. Barone, “Toward reliable density functional methods without adjustable parameters: The PBE0 model,” *The Journal of Chemical Physics* **110**, 6158–6170 (1999).
- ⁶⁷I. A. Aucar, C. A. Giménez, and G. A. Aucar, “Influence of the nuclear charge distribution and electron correlation effects on magnetic shieldings and spin-rotation tensors of linear molecules,” *RSC Advances* **8**, 20234–20249 (2018).
- ⁶⁸D. F. E. Bajac, I. A. Aucar, and G. A. Aucar, “Absolute NMR shielding scales in methyl halides obtained from experimental and calculated nuclear spin-rotation constants,” *Physical Review A* **104**, 012805 (2021).
- ⁶⁹E. O. Fischer and H. Grubert, “Über Aromatenkomplexe von Metallen, XXIX. Di-cyclopentadienyl-osmium,” *Chemische Berichte* **92**, 2302–2309 (1959).
- ⁷⁰J. C. A. Bobyens, D. C. Leventis, M. I. Bruce, and M. L. Williams, “Crystal structure of osmocene, $\text{Os}(\eta\text{-C}_5\text{H}_5)_2$,” *J. Crystallogr. Spectrosc. Res.* **16**, 519–524 (1986).
- ⁷¹M. O. Albers, D. C. Liles, D. J. Robinson, A. Shaver, E. Singleton, M. B. Wiege, J. C. A. Boeyens, and D. C. Leventis, “Chemistry of cyclopentadienylruthenium and -osmium complexes. 3. New high-yield syntheses of ruthenocenes and osmocenes. The crystal and molecular structures of decamethylruthenocene and decamethyl-osmium,” *Organometallics* **5**, 2321–2327 (1986).
- ⁷²S. K. Tokunaga, R. J. Hendricks, M. R. Tarbutt, and B. Darquié, “High-resolution mid-infrared spectroscopy of buffer-gas-cooled methyltrioxorhenium molecules,” *New Journal of Physics* **19**, 053006 (2017).
- ⁷³P. Asselin, Y. Berger, T. R. Huet, L. Margulès, R. Motiyenko, R. J. Hendricks, M. R. Tarbutt, S. K. Tokunaga, and B. Darquié, “Characterising molecules for fundamental physics: an accurate spectroscopic model of methyltrioxorhenium derived from new infrared and millimetre-wave measurements,” *Phys. Chem. Chem. Phys.* **19**, 4576–4587 (2017).
- ⁷⁴B. Darquié, N. Saleh, S. K. Tokunaga, M. Srebro-Hooper, A. Ponzi, J. Autschbach, P. Declava, G. A. Garcia, J. Crassous, and L. Nahon, “Valence-shell photoelectron circular dichroism of ruthenium(III)-tris-(acetylacetonato) gas-phase enantiomers,” *Physical Chemistry Chemical Physics* **23**, 24140–24153 (2021).
- ⁷⁵A. Shelkvnikov, R. J. Butcher, C. Chardonnet, and A. Amy-Klein, “Stability of the proton-to-electron mass ratio,” *Phys. Rev. Lett.* **100**, 150801 (2008).
- ⁷⁶E. Cantin, M. Tønnes, R. L. Targat, A. Amy-Klein, O. Lopez, and P.-E. Pottie, “An accurate and robust metrological network for coherent optical frequency dissemination,” *New Journal of Physics* **23**, 053027 (2021).
- ⁷⁷<https://www.refimeve.fr/en/homepage/>.
- ⁷⁸B. Chanteau, O. Lopez, W. Zhang, D. Nicolodi, B. Argence, F. Auguste, M. Abgrall, C. Chardonnet, G. Santarelli, B. Darquié, Y. Le Coq, and A. Amy-Klein, “Mid-infrared laser phase-locking to a remote near-infrared frequency reference for high-precision molecular spectroscopy,” *New Journal of Physics* **15**, 073003 (2013).
- ⁷⁹B. Argence, B. Chanteau, O. Lopez, D. Nicolodi, M. Abgrall, C. Chardonnet, C. Daussy, B. Darquié, Y. Le Coq, and A. Amy-Klein, “Quantum cascade laser frequency stabilization at the sub-Hz level,” *Nature Photonics* **9**, 456–460 (2015).
- ⁸⁰R. Santagata, D. B. A. Tran, B. Argence, O. Lopez, S. K. Tokunaga, F. Wiotte, H. Mouhamad, A. Goncharov, M. Abgrall, Y. Le Coq, H. Alvarez-Martinez, R. Le Targat, W. K. Lee, D. Xu, P.-E. Pottie, B. Darquié, and A. Amy-Klein, “High-precision methanol spectroscopy with a widely tunable SI-traceable frequency-comb-based mid-infrared QCL,” *Optica* **6**, 411 (2019).
- ⁸¹D. B. A. Tran, O. Lopez, M. Manceau, A. Goncharov, M. Abgrall, H. Alvarez-Martinez, R. Le Targat, E. Cantin, P.-E. Pottie, A. Amy-Klein, and B. Darquié, “Near- to mid-IR spectral purity transfer with a tunable frequency comb: Methanol frequency metrology over a 1.4 GHz span,” *APL Photonics* **9**, 030801 (2024).
- ⁸²D. B. A. Tran, M. Manceau, O. Lopez, A. Goncharov, A. Amy-Klein, and B. Darquié, “Extending frequency metrology to increasingly complex molecules: SI-traceable sub-Doppler mid-IR spectroscopy of trioxane,” (2025), [arXiv:2502.08201 \[physics\]](https://arxiv.org/abs/2502.08201).
- ⁸³M. Manceau, T. E. Wall, H. Philip, A. Baranov, O. Lopez, M. R. Tarbutt, R. Teissier, and B. Darquié, “Demonstration and frequency noise characterization of a 17 μm quantum cascade laser,” *Laser & Photonics Reviews* **20**, e00879 (2026).
- ⁸⁴Y. Wang, J. Rodewald, O. Lopez, M. Manceau, B. Darquié, B. E. Sauer, and M. R. Tarbutt, “Wavelength modulation laser spectroscopy of N₂O at 17 μm ,” *New Journal of Physics* **27**, 023038 (2025).
- ⁸⁵C. Thierfelder, P. Schwerdtfeger, and T. Saue, “⁶³Cu and ¹⁹⁷Au nuclear quadrupole moments from four-component relativistic density-functional calculations using correct long-range exchange,” *Phys. Rev. A* **76**, 034502 (2007).
- ⁸⁶A. D. Becke, “Density-functional thermochemistry. III. The role of exact exchange,” *The Journal of Chemical Physics* **98**, 5648–5652 (1993).
- ⁸⁷C. Lee, W. Yang, and R. G. Parr, “Development of the Colle-Salvetti correlation-energy formula into a functional of the electron density,” *Phys. Rev. B* **37**, 785–789 (1988).
- ⁸⁸S. H. Vosko, L. Wilk, and M. Nusair, “Accurate spin-dependent electron liquid correlation energies for local spin density calculations: a critical analysis,” *Canadian Journal of Physics* **58**, 1200–1211 (1980).
- ⁸⁹P. J. Stephens, F. J. Devlin, C. F. Chabalowski, and M. J. Frisch, “Ab initio calculation of vibrational absorption and circular dichroism spectra using density functional force fields,” *The Journal of Physical Chemistry* **98**, 11623–11627 (1994).

- ⁹⁰J. P. Perdew, K. Burke, and M. Ernzerhof, "Generalized gradient approximation made simple," *Phys. Rev. Lett.* **77**, 3865–3868 (1996).
- ⁹¹P. Hohenberg and W. Kohn, "Inhomogeneous electron gas," *Phys. Rev.* **136**, B864–B871 (1964).
- ⁹²L. Bellarosa and F. Zerbetto, "Enantiomeric excesses and electronic chirality measure," *Journal of the American Chemical Society* **125**, 1975–1979 (2003).
- ⁹³Aucar, J. J.; Stroppa, A.; Aucar, G. A. (2024). PyECM24 (v0.2.1). Zenodo. Available at <https://doi.org/10.5281/zenodo.10672183>.
- ⁹⁴J. J. Aucar, A. Stroppa, and G. A. Aucar, "A relationship between the molecular parity-violation energy and the electronic chirality measure," *The Journal of Physical Chemistry Letters* **15**, 234–240 (2023).
- ⁹⁵R. A. Hegstrom, "Electron chirality," *Journal of Molecular Structure: THEOCHEM* **232**, 17–21 (1991).
- ⁹⁶K. Fægri and T. Saue, "Diatomic molecules between very heavy elements of group 13 and group 17: A study of relativistic effects on bonding," *The Journal of Chemical Physics* **115**, 2456–2464 (2001).
- ⁹⁷S. Dubillard, J.-B. Rota, T. Saue, and K. Faegri, "Bonding analysis using localized relativistic orbitals: Water, the ultrarelativistic case and the heavy homologues H₂X (X=Te, Po, eka-Po)," *The Journal of Chemical Physics* **124**, 154307 (2006).
- ⁹⁸J. Eills, J. W. Blanchard, L. Bougas, M. G. Kozlov, A. Pines, and D. Budker, "Measuring molecular parity nonconservation using nuclear-magnetic-resonance spectroscopy," *Physical Review A* **96**, 042119 (2017).